ADVANCED ENERGY MATERIALS
www.advenergymat.de

Fine-Tuning Li-Ion Solvation Structure by Enhanced Solvent-Diluent Interactions for Long-Cycling Lithium Metal Batteries

*Guo-Xing Li, Xingyi Lyu, Au Nguyen, Rong Kou, Christy George, Siyu Wu, Ruipeng Li, Ke Wang, Tao Li, and Donghai Wang**

Achieving durable lithium (Li) metal anodes in liquid electrolytes remains challenging, primarily due to the instability of the formed solid-electrolyte interphases (SEIs). Modulating the Li-ion solvation structures is pivotal in forming a stable SEI for stabilizing Li metal anodes. Here a strategy is developed to fine-tune the Li-ion solvation structures through enhanced dipole–dipole interactions between the Li-ion-coordinated solvent and the non-Li-ion-coordinating diluent, for creating a stable SEI in the developed binary salt electrolyte. The enhanced dipole–dipole interactions weaken the coordination between Li-ions and the solvents while strengthening the interaction between Li-ions and dual anions, thereby facilitating the Li-ion transport and a robust anion-derived SEI with a distinct bilayer structure. Consequently, the developed electrolyte exhibited exceptional electrochemical performance in high energy-density Li||$LiNi_{0.8}Mn_{0.1}Co_{0.1}O_2$ (NMC811) cells, with long calendar life, stable cyclability at 1 C, and reliable operation between 25 and −20 °C, and it also demonstrat remarkable cycling stability for a Li||NMC811 pouch cell with projected energy density of 402 Wh kg^{-1}, maintaining 80% capacity retention over 606 cycles under practical conditions.

1. Introduction

Lithium (Li) metal is regarded as an ideal anode material for next-generation rechargeable batteries due to its high theoretical capacity and low density.[1,2] However, the implementation of Li metal anodes under practical conditions has been largely unachievable, because of the intrinsic reactivity of Li metal and the instability of the solid-electrolyte interphase (SEI) layer, leading to fast depletion of electrolytes, uncontrollable formation of mossy/dendritic Li metal and even safety concerns under practical operation.[3,4] To stabilize the Li metal anodes, liquid electrolyte engineering has been considered as a feasible strategy by tuning the solvation structures of Li-ions, potentially generating a stable SEI layer on the surface of Li metal anode,[5–7] thus enhancing the electrochemical performance of Li metal batteries (LMBs).

Recent advancements in electrolyte engineering have introduced diverse approaches, including high-concentration electrolytes (HCEs),[8–10] localized high-concentration electrolytes (LHCEs),[11–13] all-fluorinated electrolytes,[14,15] dual-salt carbonate electrolytes,[16,17] as well as the emerging formulated electrolyte including fluorinated orthoformate-based electrolyte,[18]

G.-X. Li, R. Kou, D. Wang
Department of Mechanical Engineering
The Pennsylvania State University
University Park, PA 16802, USA
E-mail: donghaiwang@smu.edu

X. Lyu, T. Li
Department of Chemistry and Biochemistry
Northern Illinois University
DeKalb, IL 60115, USA

A. Nguyen
Department of Materials Science and Engineering
The Pennsylvania State University
University Park, PA 16802, USA

The ORCID identification number(s) for the author(s) of this article can be found under https://doi.org/10.1002/aenm.202405680

DOI: 10.1002/aenm.202405680

R. Kou, D. Wang
Department of Mechanical Engineering
Southern Methodist University
Dallas, TX 75205, USA

C. George
Department of Chemistry
The Pennsylvania State University
University Park, PA 16802, USA

S. Wu, R. Li
National Synchrotron Light Source II (NSLS-II)
Brookhaven National Laboratory
Upton, NY 11973, USA

K. Wang
Materials Research Institute
The Pennsylvania State University
University Park, PA 16802, USA

T. Li
X-Ray Science Division
Argonne National Laboratory
Lemont, IL 60439, USA

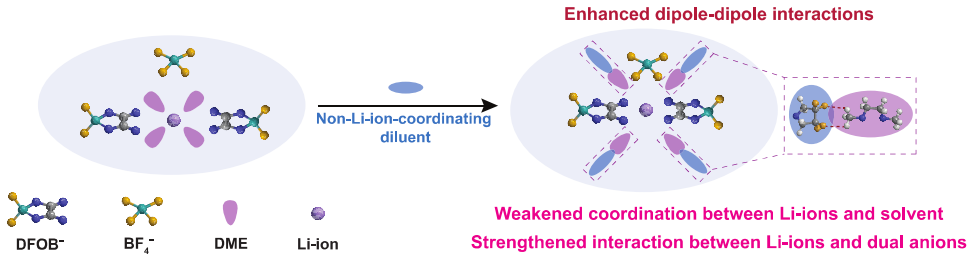

Figure 1. Schematic illustration of the tuned Li-ion solvation structure by enhanced dipole–dipole interactions between Li-ion-coordinated solvent and non-Li-ion-coordinating diluent in the binary salt electrolyte.

partially fluorinated ether-based electrolytes,[19–22] trioxane-based electrolyte[23] and asymmetric ether-like lithium salt carbonate electrolyte,[24] aiming to generate a stable SEI for stabilizing Li metal anodes. Among these advances, LHCEs have demonstrated wide effectiveness in enhancing the electrochemical performance of LMBs by introducing fluorinated ether diluents.[25] However, a persistent challenge remains in achieving long and reliable cycling performance for LMBs in LHCEs, due to the vulnerability of the formed SEIs. This vulnerability arises from the persistent degradation caused by the subtle yet continuous electrochemical decomposition of electrolyte organic solvents and diluents during cycling, which steadily undermines the robustness of the SEIs.[26] Recent study indicated that this degradation of organic solvents/diluents stems from the impaired Li-ion solvation structures and the release of free solvents stemming from the intractable dipole–dipole interactions between Li-ion coordinated solvents and polar fluorinated ether diluents within LHCEs.[27] More recently, several studies have further elegantly explored the role of these interactions in advancing electrolyte development for LMBs.[28–30] Even through these pioneering explorations, the regulation of dipole–dipole interactions is still largely unachievable. Therefore, fine-tuning these interactions could be a promising approach to regulating Li-ion solvation structures, thereby facilitating the formation of stable SEIs and stabilizing Li metal anodes.

Here we report a strategy to develop high-performance electrolytes by modulating the dipole–dipole interaction between Li-ion coordinated solvents and non-Li-ion-coordinating cyclic fluorinated ether diluents. The non-Li-ion-coordinating cyclic fluorinated ether diluent fosters an enhanced dipole–dipole interaction with the Li-ion-coordinated solvent, therefore greatly altering the solvation structures of Li-ions (**Figure 1**). This leads to the weakened coordination of Li-ions with the solvents while promoting intensified interaction between Li-ions and anions, facilitating the formation of a stable inorganic SEI layer. In this study, the synthesized cyclic fluorinated ether diluent 3,3,4,4-tetrafluorotetrahydrofuran (TFTHF) with non-coordinating capability toward Li-ions, fosters an enhanced C—F···H—C dipole–dipole interaction with the Li-ion coordinated solvent dimethoxyethane (DME), facilitating the formation of dual anion-derived inorganic-dominant SEI comprising a bilayer structure with an outer layer predominantly composed of LiF and an inner layer primarily consisting of Li_2O. The developed binary salt electrolyte not only enables unprecedented cycling stability for Li||$LiNi_{0.8}Mn_{0.1}Co_{0.1}O_2$ (NMC811) full cells with high-loading cathodes (4.0 and 5.0 mAh cm^{-2}) at room temperature and even −20 °C, but also significantly enhances calendar life of Li ||NMC811 full cells, retaining 80% capacity retention over 292 days. Furthermore, the developed electrolyte enables 80% capacity retention over 606 cycles for a 402 Wh kg^{-1} Li||NMC811 pouch cell.

2. Results and Discussion

2.1. Coordination Interactions of Solvents and Diluents with Li-Ions

The Li-ion solvation structure plays a pivotal role in dictating the SEI formation process. The solvated Li-ions undergo electrochemical reduction on the Li metal anode surface, accompanied by the decomposition of the Li-ion coordinating solvents/cosolvents and anions to form the SEI. The aforementioned electrochemical decomposition of the Li-ion coordinating solvents/cosolvents produces organic species within the SEI layer, potentially undermining the stability of the formed SEI upon cycling. Therefore, exploring the solvents/cosolvents coordination behaviors with Li-ions is essential for creating a stable SEI to stabilize the Li metal anodes.

To elucidate the coordination interactions between Li-ions and the solvent DME, as well as fluorinated ether diluents bis(2,2,2-trifluoroethyl) ether (BTFE), 1,1,2,2-tetrafluoroethyl-2,2,3,3-tetrafluoropropyl ether (TTE), and TFTHF within the binary salt electrolytes (BTFE-E: 1 M LiDFOB and 0.4 M $LiBF_4$ in DME/BTFE; TTE-E: 1 M LiDFOB and 0.4 M $LiBF_4$ in DME/TTE; and TFTHF-E: 1 M LiDFOB and 0.4 M $LiBF_4$ in DME/TFTHF), we first utilized the ^{1}H diffusion-ordered spectroscopy (DOSY) nuclear magnetic resonance (NMR) technique. For the ^{1}H DOSY NMR characterization, toluene was selected as an internal reference due to its exceptionally low coordination capability to Li-ions.[31] In principle, when the diffusion coefficient of a solvent approaches that of the internal reference toluene, it indicates diminished coordination between the solvent and Li-ions, similar as toluene of exceptionally low Li-ion coordination within the electrolyte solution. As depicted in **Figure 2**a,d,g, the diffusion coefficients of DME and BTFE decrease after 1 M LiDFOB and 0.4 M $LiBF_4$ are added and dissolved in a mixture of DME and BTFE. The diffusion coefficients of DME (2.59×10^{-9} m^2 s^{-1}) and BTFE (2.23×10^{-9} m^2 s^{-1}) decrease significantly to 0.58×10^{-9} and 1.17×10^{-9} m^2 s^{-1}, respectively, while the internal reference toluene shows a distinctly higher diffusion coefficient of 1.62×10^{-9} m^2 s^{-1} in the BTFE-E electrolyte. Similarly, the diffusion coefficients of DME and TTE are also affected by the Li salts

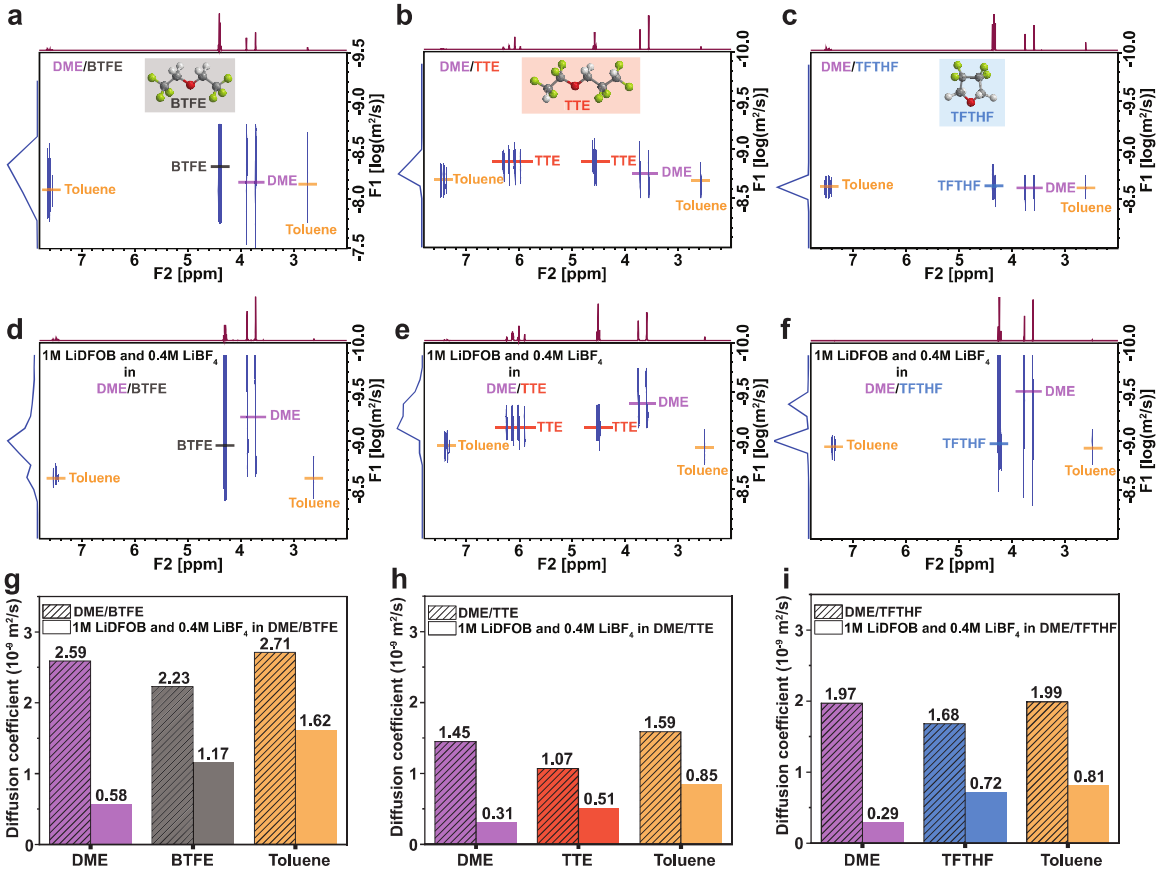

Figure 2. Coordination behaviors of solvents and diluents with Li-ions within the binary salt electrolytes. ^{1}H DOSY NMR spectra of a) DME/BTFE, b) DME/TTE, c) DME/TFTHF mixtures, and d) BTFE-E, e) TTE-E, f) TFTHF-E electrolytes. Diffusion coefficients of the solvents and diluents with and without the Li salts dissolution into the mixtures of g) DME/BTFE, h) DME/TTE, and i) DME/TFTHF. Toluene was used as the internal reference.

dissolution. As depicted in Figure 2b,e,h, the diffusion coefficients of DME (1.45×10^{-9} m^2 s^{-1}) and TTE (1.07×10^{-9} m^2 s^{-1}) significantly decrease to 0.31×10^{-9} and 0.51×10^{-9} m^2 s^{-1}, respectively, while the internal reference toluene exhibits an apparently higher diffusion coefficient of 0.85×10^{-9} m^2 s^{-1} in the TTE-E electrolyte. Notably, the diffusion coefficients of DME (1.97×10^{-9} m^2 s^{-1}) and TFTHF (1.68×10^{-9} m^2 s^{-1}) decrease to 0.29×10^{-9} and 0.72×10^{-9} m^2 s^{-1}, respectively, upon the dissolution of Li salts (Figure 2c,f,i). Interestingly, the diffusion coefficients of TFTHF and the internal reference toluene (0.81×10^{-9} m^2 s^{-1}) are very similar in the TFTHF-E electrolyte, suggesting the non-Li-ion-coordinating feature of diluent TFTHF. Collectively, the ^{1}H DOSY NMR results indicate that DME predominantly solvates Li-ions in BTFE-E, TTE-E, and TFTHF-E electrolytes, with BTFE and TTE exhibiting appreciable coordination with Li-ions, consistent with our recent findings,[32] while TFTHF shows no Li-ion coordination.

2.2. Enhanced Dipole–Dipole Interactions and Electrolyte Solvation Nanostructures

After the elucidation on the coordination interactions within the binary salt electrolytes by ^{1}H DOSY NMR characterization, we tried to further verify the non-coordinating capability of diluent TFTHF by using ^{17}O and ^{19}F NMR techniques. As depicted in **Figure 3**a and Figures S7–S9 (Supporting Information), the ^{17}O chemical shifts of the O atom in TFTHF exhibited a negligible difference (0.03 ppm) after the dissolution of Li salts LiDFOB and $LiBF_4$, confirming that the O atom in TFTHF hardly coordinates with Li-ions in the electrolyte of TFTHF-E. Interestingly, the ^{19}F NMR analysis revealed an apparent downfield shift of 0.11 ppm for the F atoms in TFTHF upon the binary Li salts dissolution (Figure 3b; Figures S10–S12, Supporting Information), seemingly contradicting the non-Li-ion coordination of the diluent TFTHF as revealed by the ^{1}H DOSY NMR analysis. This is presumably attributed to the potential dipole–dipole interaction between the F atoms in TFTHF and positively charged species, specifically the Li-ion-coordinated solvent DME, rather than the Li-ions as supported by the ^{1}H DOSY NMR characterization. To substantiate this hypothesis, the 2D ^{1}H-^{19}F heteronuclear Overhauser spectroscopy (HOESY) technique was next utilized to explore the dipole–dipole interaction between the Li-ion coordinated solvent DME and diluent TFTHF (Figure 3c,d). Given the inherent correlation between the H atoms (H_α) and F atoms (F_β) within the same TFTHF molecule (as shown in the insets of Figures 3c,d), the intensity of this H_α-F_β correlation is used as a reference and set to 1.00. There is only a

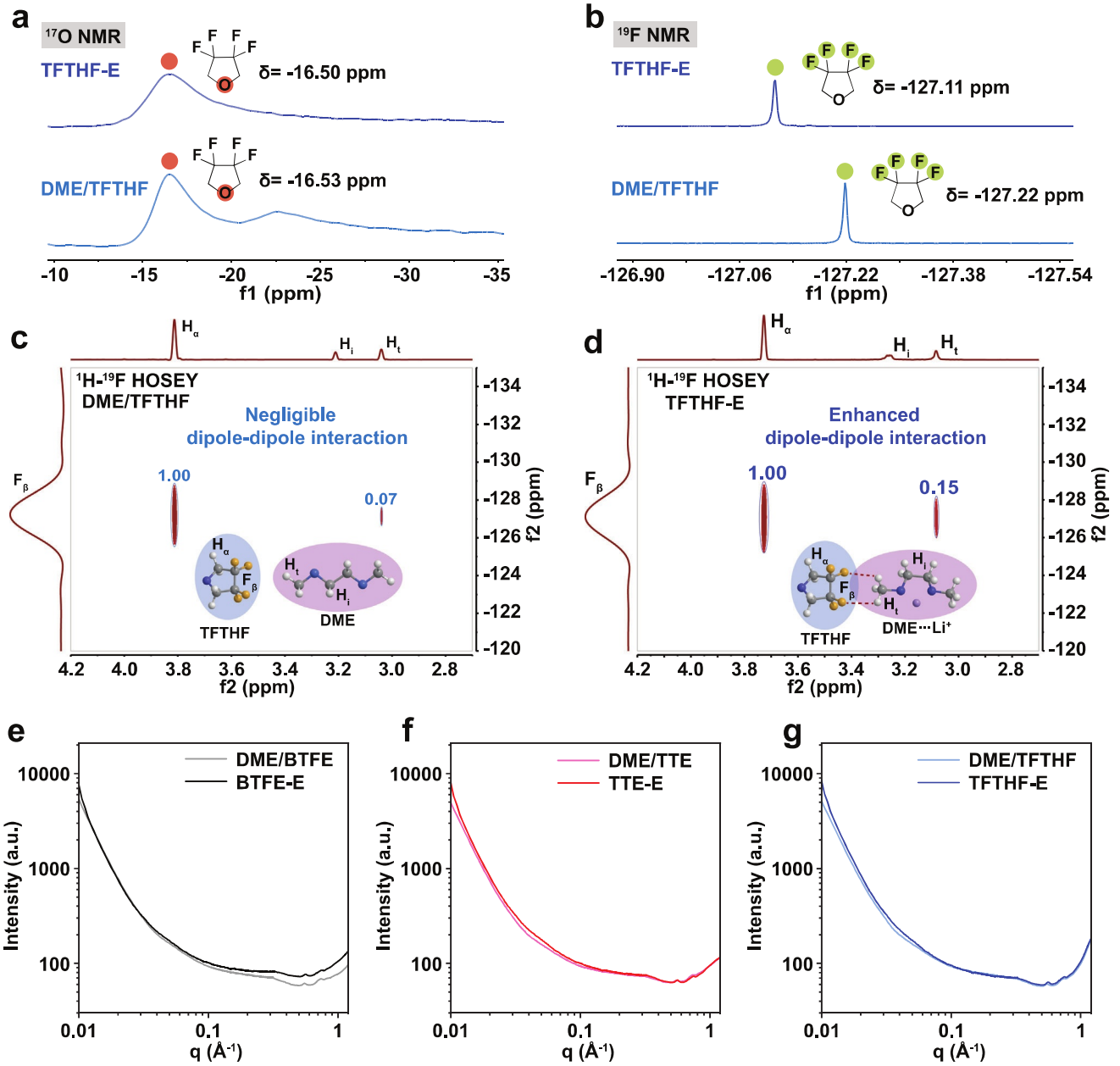

Figure 3. Enhanced dipole–dipole interactions and nanostructures of the binary salt electrolytes. a) ^{17}O and b) ^{19}F NMR characterization on the coordination behaviors of diluent TFTHF within the mixture of DME/TFTHF and electrolyte of TFTHF-E. 2D ^{1}H-^{19}F HOESY analysis of the dipole–dipole interactions between solvent DME and diluent TFTHF within the mixture of c) DME/TFTHF, d) electrolyte of TFTHF-E. SAXS analysis of the nanostructures in mixtures of e) DME/BTFE, f) DME/TTE, and g) DME/TFTHF, with and without the dual Li salts dissolution.

negligible correlation, with an intensity of 0.07, between the H atoms (labeled as H_t) at the terminal methyl group in DME and the F_β atoms in TFTHF within the DME/TFTHF mixture (Figure 3c). In contrast, a notably stronger correlation intensity of 0.15 was observed between the H_t atoms in the solvent DME and the F_β atoms in TFTHF within the TFTHF-E electrolyte (Figure 3d), confirming apparently enhanced C—F···H—C dipole–dipole interactions between the Li-ion-coordinated solvent DME and diluent TFTHF. These enhanced dipole–dipole interactions can enable weakened coordination between Li-ions and solvent DME while intensifying interactions between Li-ions and anions, thereby promising homogeneous solvation nanostructures, improved Li-ion transference number (T_{Li^+}) and the formation of an anion-derived SEI in the electrolyte of TFTHF-E,[33] as will be elaborated in detail in the following sections.

To explore the impact of enhanced dipole–dipole interactions on the solvation nanostructures of the binary salt electrolytes, the small-angle X-ray scattering (SAXS) technique was applied, due to its effectiveness in studying the long-range solvation structures such as cluster or aggregate of battery liquid electrolytes.[34,35] The

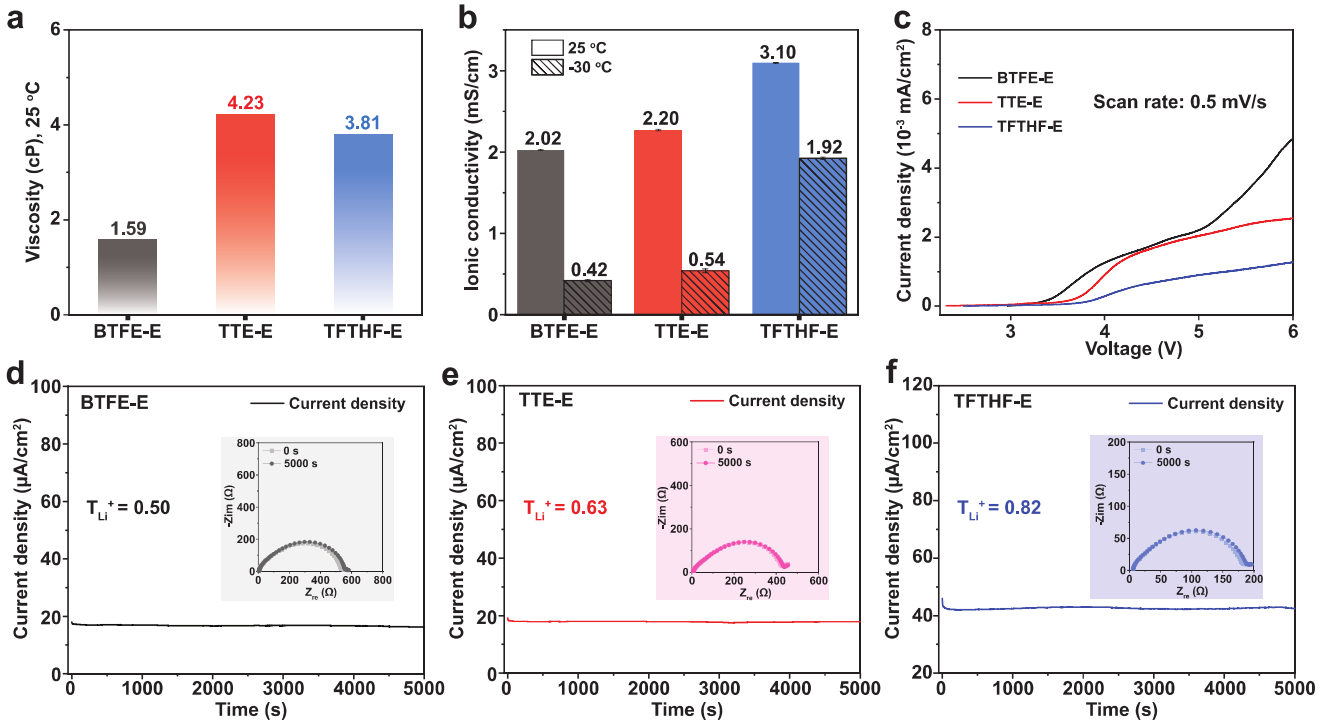

Figure 4. Physicochemical properties of the binary salt electrolytes. a) Viscosities of BTFE-E, TTE-E, and TFTHF-E electrolytes at 25 °C. b) Ionic conductivities of BTFE-E, TTE-E, and TFTHF-E electrolytes at 25 and −30 °C. c) LSV of BTFE-E, TTE-E, and TFTHF-E electrolytes in Li||Al cells. Li-ion transference number measurement of d) BTFE-E, e)TTE-E, and f) TFTHF-E electrolytes using Li||Li symmetric cells, with the EIS spectra before and after the polarization as the insets.

SAXS profiles of the electrolytes of BTFE-E, TTE-E, and TFTHF-E were collected and assessed against those of the corresponding pure solvent/diluent mixtures, as shown in Figure 3e–g. For BTFE-E electrolytes, a pronounced intensity increase was observed in the q range of 0.1–1.1 $Å^{-1}$ when compared to the mixture of DME/BTFE.[36] In contrast, for the TTE-E and TFTHF-E electrolytes, the intensity remains nearly unchanged, indicating that these two electrolytes maintain greater homogeneity upon Li salts addition and support the homogeneous solvation nanostructures in the developed TFTHF-E electrolyte.

2.3. Physicochemical and Electrochemical Properties of Binary Salt Electrolytes

The viscosities of the binary salt electrolytes of BTFE-E, TTE-E, and TFTHF-E were measured at 25 °C, as shown in **Figure** 4a. TFTHF-E exhibited a moderate viscosity of 3.81 cP. Additionally, the introduction of the cyclic fluorinated ether diluent TFTHF significantly enhanced ionic conductivity (Figure 4b), with the TFTHF-E electrolyte demonstrating a conductivity of 3.10 mS cm^{-1} at 25 °C and maintaining 1.92 mS cm^{-1} at −30 °C, underscoring its potential viability under low-temperature conditions. In contrast, both BTFE-E and TTE-E electrolytes showed inferior ionic conductivities at both 25 and −30 °C.

The electrolytes' oxidation stability was evaluated using linear sweep voltammetry (LSV) on Li||Al cells at a scan rate of 0.5 mV s^{-1}, as depicted in Figure 4c. The BTFE-E and TTE-E electrolytes exhibit inferior oxidation stability with oxidation potentials ≈4.0 and 4.2 V (vs Li^+/Li), respectively, when the oxidation current density reaches 1.3 μA cm^{-2}. Notably, the TFTHF-E electrolyte demonstrates a substantially enhanced oxidation stability window exceeding 6 V, with an oxidation current density reaching 1.3 μA cm^{-2}. The enhanced stability of TFTHF-E electrolyte against oxidation can be attributed to the introduction of the non-coordinating diluent TFTHF, which barely coordinates with Li ions, thereby mitigating the release of free DME solvent.

Based on the 2D ^1H-^{19}F HOESY analysis, an enhanced dipole–dipole interaction between diluent TFTHF and the Li-ion-coordinated DME was observed, promising an improved T_{Li}^+ in the developed electrolyte of TFTHF-E. The T_{Li}^+ values of BTFE-E, TTE-E, and TFTHF-E electrolytes were then measured by following a reported testing protocol,[37] as illustrated in Figure 4d–f. The developed electrolyte of TFTHF-E exhibited a significantly higher T_{Li}^+ value of 0.82, in contrast to the lower T_{Li}^+ values of 0.50 and 0.63 for electrolytes of BTFE-E and TTE-E, respectively. This elevated T_{Li}^+ not only potentially accelerates Li-ion transfer kinetics, but also facilitates enhanced Li metal reversibility in the electrolyte of TFTHF-E.[38] To validate the Li metal plating/stripping reversibility in TFTHF-E electrolyte, Coulombic efficiencies (CEs) of anode-free Cu||NMC811 cells were measured (Figure S13, Supporting Information). The TFTHF-E electrolyte demonstrates a notable improvement, achieving the highest average CE of 99.6%, in comparison to the BTFE-E and TTE-E electrolytes, which exhibit inferior average CEs of 99.0% and 99.1%, respectively.

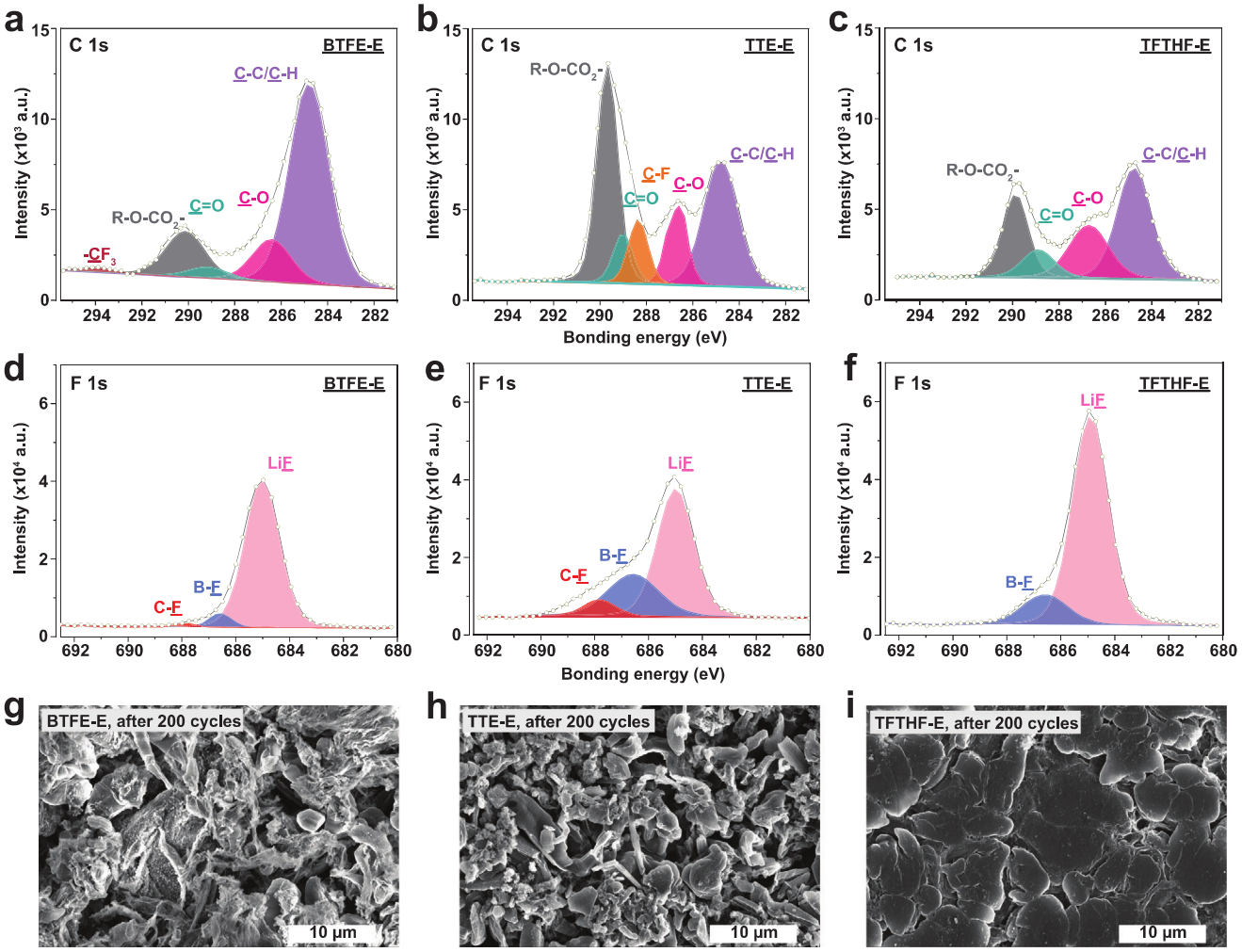

Figure 5. Chemical composition analysis of the SEIs and Li metal anode morphologies. High-resolution C 1s and F 1s XPS spectra of the formed SEIs in a–d) BTFE-E, b–e) TTE-E, and c–f) TFTHF-E electrolytes. SEM images of Li metal anode after 200 cycles in Li||NMC811 cells in g) BTFE-E, h) TTE-E, and i) TFTHF-E electrolytes.

2.4. SEIs Chemical Compositions and Lithium Metal Morphologies

The formed SEIs were analyzed using X-ray photoelectron spectroscopy (XPS) on cycled Li metal anodes to reveal their interfacial chemical compositions. As shown in **Figure** 5a,b, high-resolution XPS spectra of C 1s identify the presence of $-CF_3$ (≈293.8 eV) and C—F (≈288.4 eV) within the SEIs formed in BTFE-E and TTE-E, confirming the electrochemical decomposition of cosolvents BTFE and TTE during cycling. This decomposition was further verified by the high-resolution F 1s XPS spectra (Figure 5d,e) which show peaks at ≈688.0 eV for C—F bonds, indicating the decomposition of BTFE and TTE during SEI formation. The electrochemical decomposition of BTFE and TTE can be attributed to their coordination to Li-ions, as revealed by the ^{1}H DOSY NMR results in Figure 2. In contrast, the non-coordinating diluent TFTHF demonstrates excellent electrochemical stability against Li metal anode, as evidenced by the absence of detectable C—F decomposition in the formed SEI, confirmed by high-resolution C 1s and F 1s XPS analyses (Figure 5c–f).

To further reveal the composition distribution within the formed SEIs, the depth profiles of organic species, Li_2O and LiF, were obtained from the XPS depth profiling results. Both BTFE-E and TTE-E electrolytes facilitate SEIs with an outer layer rich in organic components and an inner layer dominated by Li_2O (Figure S20a,b, Supporting Information). In contrast, the TFTHF-E electrolyte promotes an inorganic-dominant SEI layer, with an outer layer enriched with LiF and an inner layer enriched with Li_2O (Figure S20c, Supporting Information). Overall, the XPS data indicate that the TFTHF-E electrolyte promotes a robust SEI, characterized by an outer layer predominantly composed of LiF and an inner layer primarily consisting of Li_2O. This formed bilayer SEI can promote uniform Li deposition and mitigate side reactions of Li metal anodes, as revealed by the scanning electron microscope (SEM) studies in Figure 5g–i and Figure S21 (Supporting Information).

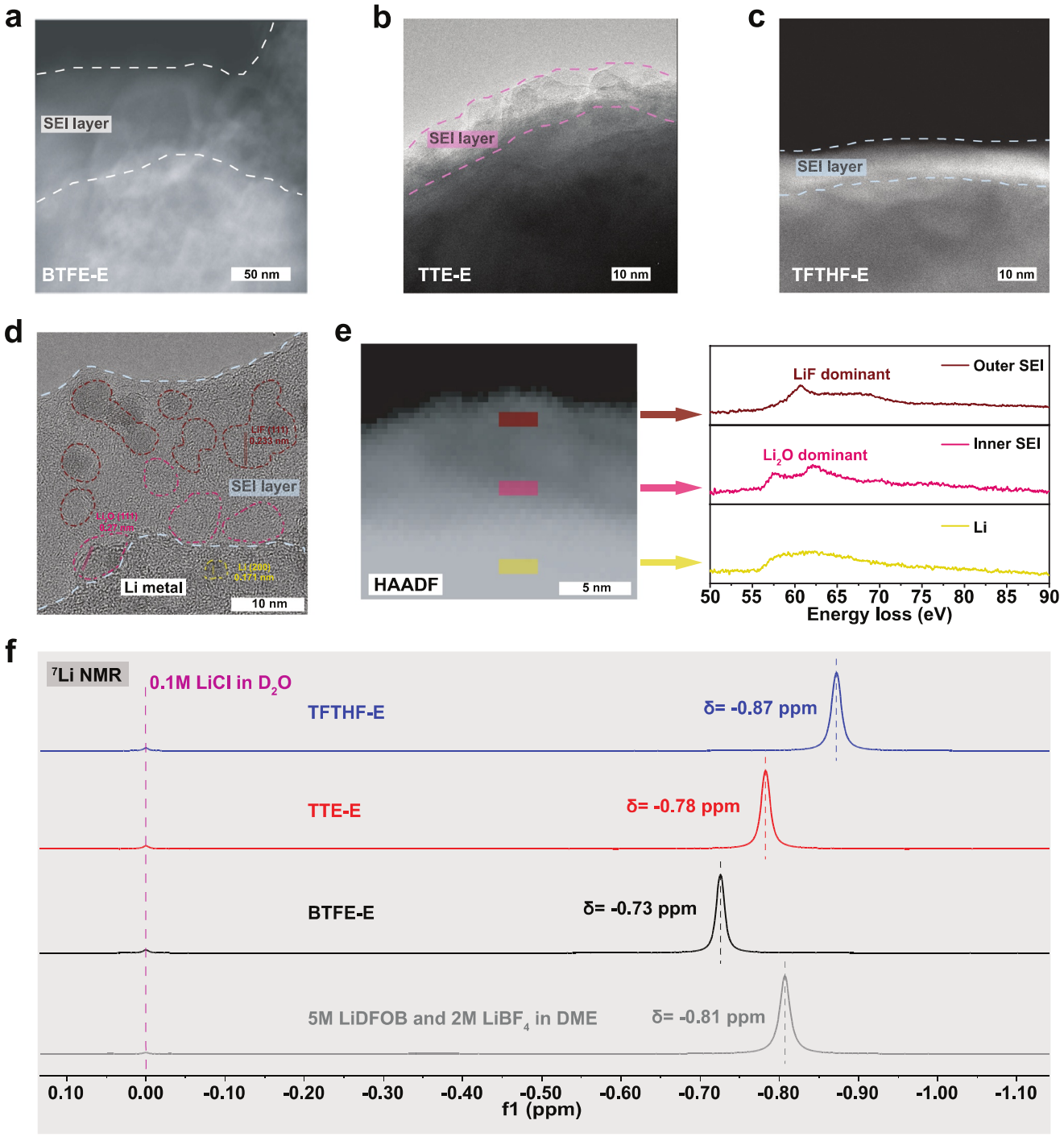

Figure 6. SEI nanostructures and the enhanced Li-ion-anion interactions. Cryo-TEM images of the formed SEIs in a) BTFE-E, b) TTE-E, and c) TFTHF-E electrolytes. d) High-resolution TEM image, e) HAADF-TEM image, and Li K-edge EELS spectra of the formed SEI in TFTHF-E electrolyte. f) ^{7}Li NMR analysis on the solvation structures of Li-ions in the binary salt electrolytes.

2.5. SEI Nanostructures and Intensified Lithium-Ion Coordination with Anions

The nanostructures of the SEIs were further explored using the cryogenic transmission electron microscopy (cryo-TEM) technique. The formed SEI layer in BTFE-E is notably thick (≈80 nm), and primarily consists of an amorphous structure (**Figure 6a**). Similarly, the formed SEI layer in TTE-E also displays a predominantly amorphous structure, though it is thinner at ≈20 nm (Figure 6b). In contrast, the formed SEI in TFTHF-E appears thin, with a thickness of ≈20 nm, and is featured by a dense and uniform structure (Figure 6c). A high-resolution cryo-TEM

image of the TFTHF-E facilitated SEI was captured, as depicted in Figure 6d. The LiF {111} plane featuring a 0.233 nm lattice spacing (within the maroon-outlined region) and the Li_2O {111} plane featuring a 0.27 nm lattice spacing (within the pink-outlined region) were observed within the formed SEI layer, along with the Li {200} plane featuring a 0.171 nm lattice spacing (within the yellow-outlined region). A prominent bilayer-structured SEI with an outer layer predominantly composed of LiF and an inner layer primarily consisting of Li_2O was characterized, confirming the results obtained from XPS depth profiling.

The nanostructures of the formed SEI facilitated by TFTHF-E were also explored by electron energy loss spectroscopy (EELS) techniques (Figure 6e). A high-angle annular dark-field scanning transmission electron microscopy (HAADF-STEM) image was captured, and three distinct regions, marked in maroon, pink, and yellow, representing the outer SEI layer, inner SEI layer and deposited Li layer, respectively, were investigated by EELS. From the upper maroon region, the Li K-edge spectrum reveals the presence of LiF, confirming the formation of an outer SEI dominated in LiF. In the central pink region, the spectrum is consistent with Li_2O, indicating an inner SEI layer predominantly composed of Li_2O. The spectrum from the lower yellow region aligns with electrochemically deposited metallic Li. Taken together, these electron microscopic findings further confirm the creation of a distinctive bilayer SEI featuring an outer layer predominantly composed of LiF and an inner layer primarily consisting of Li_2O in the developed TFTHF-E electrolyte.

Achievement of the thin, inorganic-dominant SEI layer indicates a predominantly anion-derived SEI formation process in the TFTHF-E electrolyte. Thus, investigating the solvation structure of Li-ions can provide valuable insights into the underlying chemistry of the SEI formation process. To probe the solvation structures of Li-ions in the binary salt electrolytes, ^{7}Li NMR analysis was utilized. As illustrated in Figure 6f and Figure S22 (Supporting Information), using a solution of 0.1 M LiCl in D_2O as the internal reference ($\delta = 0$ ppm), the addition of BTFE to the pre-diluted concentrated electrolyte of 5 M LiDFOB and 2 M $LiBF_4$ in DME resulted in a downfield chemical shift from −0.81 to −0.73 ppm. The introduction of TTE caused a slight downfield shift to −0.78 ppm. These observations indicate that the addition of BTFE and TTE disrupts the pristine Li-ion solvation structures within the pre-diluted concentrated electrolyte of 5 M LiDFOB and 2 M $LiBF_4$ in DME, leading to weakened interactions between the anions $DFOB^-$ and $BF_4^-$and the Li-ions in both the BTFE-E and TTE-E electrolytes. In contrast, a detectable upfield chemical shift (−0.87 ppm) was observed following the addition of the diluent TFTHF, suggesting intensified interactions between the Li-ions and the anions $DFOB^-$ and BF_4^- within the TFTHF-E electrolyte, compared to the pre-diluted concentrated electrolyte of 5 M LiDFOB and 2 M $LiBF_4$ in DME. These enhanced Li-ion-anion interactions will facilitate the anion-derived SEI formation process in the TFTHF-E electrolyte, as elucidated by the XPS and cryo-TEM results. The creation of the bilayer SEI structure featuring an outer layer predominantly composed of LiF and an inner layer primarily consisting of Li_2O facilitated by the developed TFTHF-E electrolyte can be attributed to the stronger Li-ion coordination capability of $DFOB^-$ anions over BF_4^- anions and the resultant preferentially electrochemical decomposition for SEI formation, as reported in the literature.[32,39]

2.6. Electrochemical Performance Evaluation of Lithium Metal Batteries

After revealing the influences of enhanced dipole–dipole interactions on the chemistry of electrolyte and SEI layer, we further conducted an electrochemical evaluation of LMBs using the binary salt electrolytes of BTFE-E, TTE-E, and TFTHF-E. To evaluate the reliability of these binary salt electrolytes in stabilizing Li metal anodes under practical operation, we adopted a testing protocol that incorporated a 24-h rest interval between the charge and discharge cycles for the self-discharge evaluation (**Figure** 7a; Figure S23, Supporting Information). The developed electrolyte of TFTHF-E demonstrated 80% capacity retention after 225 cycles over 292 days for the Li||NMC811 full cells. In contrast, the cells using BTFE-E and TTE-E electrolytes experienced fast capacity loss, maintaining only 80% capacity after 51 and 65 cycles, respectively. These results indicate that the SEI layer facilitated by TFTHF-E can significantly mitigate Li metal corrosion and stabilize the Li metal anode, thus demonstrating its potential for improving the calendar life of LMBs.[40]

Due to the readily Li dendrites formation and accumulation during fast charging and operation at low temperatures, the performance of LMBs under these conditions remains challenging. Encouraged by the properties of the TFTHF-E electrolyte, including its moderated viscosity, high ionic conductivity, and Li-ion transference number, as illustrated in Figure 4, it is reasonable to deduce its feasibility of enabling fast changing of LMBs. Hence, we evaluated the cycling stability of Li ||NMC811 full cells when charging and discharging at 1C. As depicted in Figure 7b and Fgirure S24 (Supporting Information), the cells using BTFE-E and TTE-E electrolytes experienced fast decay, with capacity retention of 80% after 27 and 43 cycles, respectively. In contrast, TFTHF-E demonstrated a greatly enhanced cycling longevity, with a capacity retention of 80% after 218 cycles. Furthermore, the Li|| NMC811 full cells cycled alternately at 25 and −20 °C, and demonstrated stable cycling performance with a capacity retention of 80% after a total of 200 cycles in the TFTHF-E electrolyte (Figure 7c; Figure S27, Supporting Information). Additionally, the cycling performance of Li||NMC811 full cells at an elevated temperature of 65 °C was also assessed, delivering remarkable cycling stability with a capacity retention of 80% over 207 cycles in the TFTHF-E electrolyte (Figure 7d; Figure S28, Supporting Information). These results substantiate the promising practical application of the developed TFTHF-E electrolyte for LMBs under extreme conditions.

The cycling stability of full cell incorporated high-loading NMC811 (5.0 mAh cm^{-2}) and thin Li metal anode (20 µm) with a low electrolyte/capacity (E/C) ratio of 6 µL mAh^{-1}, was further evaluated in the electrolyte of TFTHF-E (Figure 7e; Figure S29, Supporting Information). The cell demonstrated notable cycling stability, delivering a capacity retention of 80% over 445 cycles. Additionally, the Li||NMC811 full cell incorporated cathode with the areal capacity of 4.0 mAh cm^{-2} and 50 µm-thickness Li metal anode, demonstrated an exceptional cycling performance with a capacity retention of 80% over 600 cycles in TFTHF-E, compared to electrolytes of BTFE-E and TTE-E (Figure 7f; Figure S30, Supporting Information). Furthermore, a double-layer Li||NMC811 pouch cell with a projected gravimetric energy density of 402 Wh kg^{-1} (Table S1, Supporting

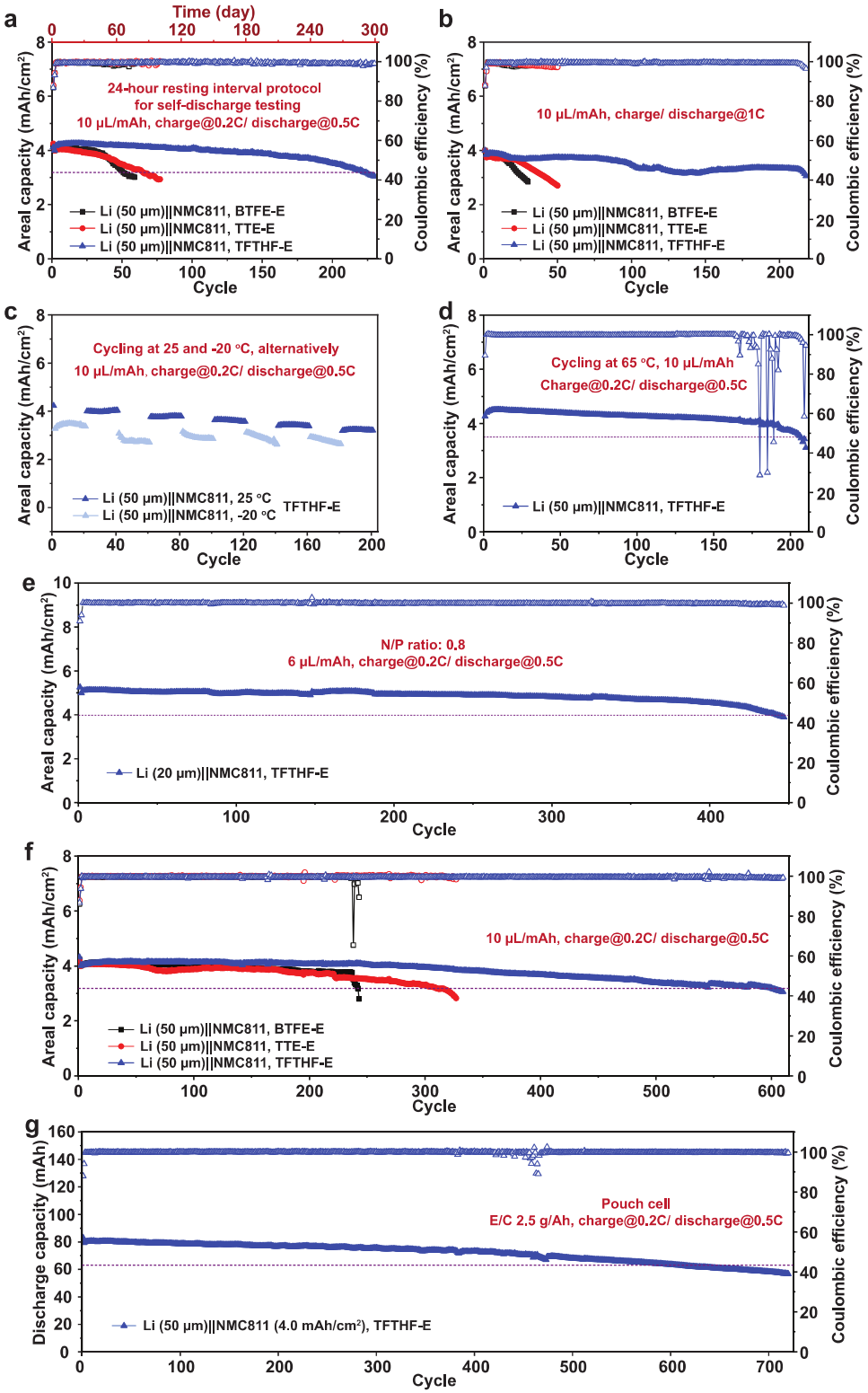

Figure 7. Electrochemical evaluation of Li||NMC811 cells in the binary salt electrolytes. a) Self-discharge evaluation of Li||NMC811 cells. b) Fast charge and discharge at 1C of Li||NMC811 cells. c) Cycling stability of Li||NMC811 cells in TFTHF-E at 25 and −20 °C, alternatively. d) Cycling stability of Li||NMC811 cells in TFTHF-E at 65 °C. e) Cycling stability of the Li (20 μm)||NMC811 (5 mAh cm^{-2}) cell in TFTHF-E. f) Cycling stability of Li||NMC811 cells at room temperature. g) Cycling stability of Li||NMC811 pouch cell under practical conditions in TFTHF-E.

Information) was fabricated to examine the practicality of TFTHF-E electrolyte. The pouch cell demonstrated state-of-the-art cycling performance in literature, offering 80% capacity retention over 606 cycles (Figures 7g; Figure S31 and Table S2, Supporting Information). Collectively, the achieved electrochemical evaluations of Li||NMC811 full cells across different demanding scenarios validate the efficacy of the developed TFTHF-E electrolyte, characterized by the enhanced dipole–dipole interactions between Li-ion coordinated DME and the diluent TFTHF, in achieving stable and long-life LMBs for practical applications.

3. Conclusion

In this study, we developed a strategy for creating a stable SEI to stabilize Li metal anode by modulating dipole–dipole interactions between the solvent and diluent. The resultant enhanced dipole–dipole interactions, fostered by the non-Li-ion-coordinating diluent TFTHF, can regulate the Li-ion solvation structures, weakening the Li-ion coordination of Li-ions with solvent DME while intensifying interactions between Li-ions and dual anions. Consequently, this facilitates the Li-ion transfer kinetics and, more importantly, actively promotes the generation of a robust SEI layer, thereby significantly improving the electrochemical performance of high-energy density LMBs. This protocol demonstrates the potential and feasibility of regulating the dipole–dipole interactions between solvents and diluents, advancing the understanding of designing advanced liquid electrolytes for practical LMBs.

Supporting Information

Supporting Information is available from the Wiley Online Library or from the author.

Acknowledgements

This work was supported by the Assistant Secretary for Energy Efficiency and Renewable Energy, Office of Vehicle Technologies of the U.S. Department of Energy, through the Advanced Battery Materials Research Program (Battery500 Consortium) and Battelle-Pacific Northwest National Laboratory Subcontract Award 614551. This study utilized the facilities of the Complex Materials Scattering (CMS) beamline at the National Synchrotron Light Source II (NSLS-II), which is a US DOE Office of Science Facility located at Brookhaven National Laboratory (BNL), operating under Contract No. DE-SC0012704. T. Li is thankful for the support by the U.S. National Science Foundation (Grant No. 2342334).

Conflict of Interest

D.W. and G.X.L. are inventors on U.S. provisional patent application No. 63/632 filed by The Pennsylvania State University, which pertains to the electrolyte formulations reported in this study. D. W. has a financial interest in the company AscenPower, which is being appropriately managed by The Pennsylvania State University. The other authors declare no conflicts of interest.

Data Availability Statement

The data that support the findings of this study are available in the supplementary material of this article.

Keywords

dipole–dipole interaction, electrolyte engineering, lithium metal anodes, solid electrolyte interphase, solvation structure

Received: December 2, 2024
Revised: January 20, 2025
Published online: February 24, 2025

[1] J.-M. Tarascon, M. Armand, *Nature* **2001**, *414*, 359.
[2] M. Wittingham, *Pro. IEEE* **2012**, *100*, 1518.
[3] D. Lin, Y. Liu, Y. Cui, *Nat. Nanotechnol.* **2017**, *12*, 194.
[4] X.-B. Cheng, R. Zhang, C.-Z. Zhao, Q. Zhang, *Chem. Rev.* **2017**, *117*, 10403.
[5] K. Xu, *J. Electrochem. Soc.* **2007**, *154*, A162.
[6] E. Peled, S. Menkin, *J. Electrochem. Soc.* **2017**, *164*, A1703.
[7] S. Tan, D. Kuai, Z. Yu, S. Perez-Beltran, M. M. Rahman, K. Xia, N. Wang, Y. Chen, X.-Q. Yang, J. Xiao, J. Liu, Y. Cui, Z. Bao, P. B. Balbuena, E. Hu, *J. Am. Chem. Soc.* **2024**, *146*, 11711.
[8] J. Qian, W. A. Henderson, W. Xu, P. Bhattacharya, M. Engelhard, O. Borodin, J.-G. Zhang, *Nat. Commun.* **2015**, *6*, 6362.
[9] J. Wang, Y. Yamada, K. Sodeyama, C. H. Chiang, Y. Tateyama, A. Yamada, *Nat. Commun.* **2016**, *7*, 12032.
[10] X. Fan, L. Chen, X. Ji, T. Deng, S. Hou, J. Chen, J. Zheng, F. Wang, J. Jiang, K. Xu, C. Wang, *Chem* **2018**, *4*, 174.
[11] S. Chen, J. Zheng, D. Mei, K. S. Han, M. H. Engelhard, W. Zhao, W. Xu, J. Liu, J.-G. Zhang, *Adv. Mater.* **2018**, *30*, 1706102.
[12] X. Ren, S. Chen, H. Lee, D. Mei, M. H. Engelhard, S. D. Burton, W. Zhao, J. Zheng, Q. Li, M. S. Ding, M. Schroeder, J. Alvarado, K. Xu, Y. S. Meng, J. Liu, J.-G. Zhang, W. Xu, *Chem* **2018**, *4*, 1877.
[13] X. Ren, L. Zou, X. Cao, M. H. Engelhard, W. Liu, S. D. Burton, H. Lee, C. Niu, B. E. Matthews, Z. Zhu, C. Wang, B. W. Arey, J. Xiao, J. Liu, J.-G. Zhang, W. Xu, *Joule* **2019**, *3*, 1662.
[14] X. Fan, L. Chen, O. Borodin, X. Ji, J. Chen, S. Hou, T. Deng, J. Zheng, C. Yang, S.-C. Liou, K. Amine, K. Xu, C. Wang, *Nat. Nanotechnol.* **2018**, *13*, 715.
[15] X. Fan, X. Ji, L. Chen, J. Chen, J. Chen, T. Deng, F. Han, J. Yue, N. Piao, R. Wang, X. Zhou, X. Xiao, L. Chen, C. Wang, *Nat. Energy* **2019**, *4*, 882.
[16] R. Weber, M. Genovese, A. J. Louli, S. Hames, C. Martin, I. G. Hill, J. R. Dahn, *Nat. Energy* **2019**, *4*, 683.
[17] A. J. Louli, A. Eldesoky, R. Weber, M. Genovese, M. Coon, J. deGooyer, Z. Deng, R. T. White, J. Lee, T. Rodgers, R. Petibon, S. Hy, S. J. H. Cheng, J. R. Dahn, *Nat. Energy* **2020**, *5*, 693.
[18] X. Cao, X. Ren, L. Zou, M. H. Engelhard, W. Huang, H. Wang, B. E. Matthews, H. Lee, C. Niu, B. W. Arey, Y. Cui, C. Wang, J. Xiao, J. Liu, W. Xu, J.-G. Zhang, *Nat. Energy* **2019**, *4*, 796.
[19] Z. Yu, H. Wang, X. Kong, W. Huang, Y. Tsao, D. G. Mackanic, K. Wang, X. Wang, W. Wang, W. Huang, S. Choudhury, Y. Zheng, C. V. Amanchukwu, S. T. Hung, Y. Ma, E. G. Lomeli, J. Qin, Y. Cui, Z. Bao, *Nat. Energy* **2020**, *5*, 526.
[20] C. V. Amanchukwu, Z. Yu, X. Kong, J. Qin, Y. Cui, Z. Bao, *J. Am. Chem. Soc.* **2020**, *142*, 7393.
[21] Z. Yu, P. E. Rudnicki, Z. Zhang, Z. Huang, H. Celik, S. T. Oyakhire, Y. Chen, X. Kong, S. C. Kim, X. Xiao, H. Wang, Y. Zheng, G. A. Kamat, M. S. Kim, S. F. Bent, J. Qin, Y. Cui, Z. Bao, *Nat. Energy* **2022**, *7*, 94.
[22] G. Zhang, J. Chang, L. Wang, J. Li, C. Wang, R. Wang, G. Shi, K. Yu, W. Huang, H. Zheng, T. Wu, Y. Deng, J. Lu, *Nat. Commun.* **2023**, *14*, 1081.
[23] Q.-K. Zhang, X.-Q. Zhang, J. Wan, N. Yao, T.-L. Song, J. Xie, L.-P. Hou, M.-Y. Zhou, X. Chen, B.-Q. Li, R. Wen, H.-J. Peng, Q. Zhang, J.-Q. Huang, *Nat. Energy* **2023**, *8*, 725.

[24] Y. Xia, P. Zhou, X. Kong, J. Tian, J. Tian, W. Zhang, S. Yan, W.-H. Hou, H.-Y. Zhou, H. Dong, X. Chen, P. Wang, Z. Xu, L. Wan, B. Wang, K. Liu, *Nat. Energy* **2023**, *8*, 934.
[25] X. Cao, H. Jiao, W. Xu, J.-G. Zhang, *J. Electrochem. Soc.* **2021**, *168*, 010522.
[26] X. Cao, P. Gao, X. Ren, L. Zou, M. H. Engelhard, B. E. Matthews, J. Hu, C. Niu, D. Liu, B. W. Arey, C. Wang, J. Xiao, J. Liu, W. Xu, J.-G. Zhang, *Proc. Natl. Acad. Sci. USA* **2021**, *118*, 2020357118.
[27] F. Ren, Z. Li, J. Chen, P. Huguet, Z. Peng, S. Deabate, *ACS Appl. Mater. Interfaces* **2022**, *14*, 4211.
[28] M. Qin, M. Liu, Z. Zeng, Q. Wu, Y. Wu, H. Zhang, S. Lei, S. Cheng, J. Xie, *Adv. Energy Mater.* **2022**, *12*, 2201801.
[29] H. Zhang, Z. Zeng, S. Cheng, J. Xie, *eScience* **2024**, *4*, 100265.
[30] M. Qin, Z. Zeng, S. Cheng, J. Xie, *Acc. Chem. Res.* **2024**, *57*, 1163.
[31] C.-C. Su, M. He, R. Amine, Z. Chen, K. Amine, *Angew. Chem., Int. Ed.* **2018**, *57*, 12033.
[32] G.-X. Li, V. Koverga, A. Nguyen, R. Kou, M. Ncube, H. Jiang, K. Wang, M. Liao, H. Guo, J. Chen, N. Dandu, A. T. Ngo, D. Wang, *Nat. Energy* **2024**, *9*, 817.
[33] K. Xu, *Chem. Rev.* **2004**, *104*, 4303.
[34] X. Liu, L. Fang, X. Lyu, R. E. Winans, T. Li, *Chem. Mater.* **2023**, *35*, 9821.
[35] K. Qian, R. E. Winans, T. Li, *Adv. Energy Mater.* **2020**, *11*, 2002821.
[36] Z. Feng, E. Sarnello, T. Li, L. Cheng, *J. Electrochem. Soc.* **2019**, *166*, A47.
[37] K. M. Abraham, Z. Jiang, B. Carroll, *Chem. Mater.* **1997**, *9*, 1978.
[38] L. Suo, Y.-S. Hu, H. Li, M. Armand, L. Chen, *Nat. Commun.* **2013**, *4*, 1481.
[39] M. Mao, X. Ji, Q. Wang, Z. Lin, M. Li, T. Liu, C. Wang, Y.-S. Hu, H. Li, X. Huang, L. Chen, L. Suo, *Nat. Commun.* **2023**, *13*, 1082.
[40] X. Cao, Y. Xu, L. Zou, J. Bao, Y. Chen, B. E. Mattews, J. Hu, X. He, M. H. Engelhard, C. Niu, B. W. Arey, C. Wang, J. Xiao, J. Liu, C. Wang, W. Xu, J.-G. Zhang, *Energy Environ. Sci.* **2023**, *16*, 1548.